The Effect of Antecedent Topography on Complex Crater Formation

Don R. Hood[1]
Brennan W. Young[2]
Aviv L. Cohen-Zada[2]
Peter B. James[1]
Ryan C. Ewing[2]
Jeffery S. Lee[1]

[1] Baylor University, Department of Geoscience
[2] Texas A&M University Geology and Geophysics

Corresponding Author: Donald R Hood (drhood2938@gmail.com)

Key Points

- Overlapping complex crater rims are lower inside the antecedent basins compared to outside.
- Deeper antecedent basins and more significant crater overlap tend to create larger differences in rim height.
- Changes in the impact crater formation process, mainly during transient rim collapse, influence the shape of overlapping crater rims.

Abstract

Impact craters that form on every planetary body provide a record of planetary surface evolution. On heavily-cratered surfaces, new craters that form often overlap older craters, but it is unknown how the presence of older craters alters impact crater formation. We use overlapping complex crater pairs on the lunar surface to constrain this process and find that crater rims are systematically lower where they intersect antecedent crater basins. However, the rim morphology of the new crater depends on both the depth of the antecedent crater and the degree of overlap between the two craters. Our observations suggest that transient rim collapse is altered by antecedent topography, leading to circumferential distribution of rim materials in the younger crater. This study represents the first formalization of the influence of antecedent topography on rim morphology and provides process insight into a common impact scenario relevant to the geology of potential Artemis landing sites.

Plain Language Summary

Craters form on the surface of every planetary body and help us to understand many qualities of the surface including, critically, the age of the surface. On older surfaces with many craters, new craters that form often overlap and partially destroy older craters, though we don't know if or how the presence of the older crater changes the processes that create the new crater. Looking at large Lunar craters, we can determine that the presence of an older crater causes the rim of the new crater to be asymmetric: lower where it forms within the older crater basin. The difference in height between the new crater rim inside and outside the old crater depends on both the depth of the older crater, and where the new crater forms relative to the older crater. From this we can interpret that the presence of the older crater alters the way the new crater forms, leading to an uneven collapse of early rim materials.

1. Introduction

Impact cratering sculpts the topography of all solid planetary bodies and is singularly important on airless bodies like the Moon. The genesis of crater morphology, its evolution, and relationship to the impact process is the subject of numerous experiments (Aschauer and Kenkmann, 2017), models (Elbeshausen et al., 2009; Krohn et al., 2014; Wünnemann and Ivanov, 2003), and surveys (Robbins, 2019; Wang et al., 2021). These studies establish clear relationships between crater morphology and impact process, enabling investigations of planetary regolith (Izquierdo et al., 2021), buried ice (Bramson et al., 2015; Dundas et al., 2021), and surface age (Hartmann and Neukum, 2001) based on crater morphology and physical properties. However, impact crater models generally disregard the influence of antecedent topography in the target on the final crater shape. Studies of simple craters in high-relief terrains (Aschauer and Kenkmann, 2017; Krohn et al., 2014) demonstrate that antecedent slopes influence crater morphology, but it is frequently assumed that complex craters obliterate the underlying topography (Hirabayashi et al., 2017; Riedel et al., 2020). Martian craters that straddle the topographic dichotomy, such as Gale Crater (Schwenzer et al., 2012) and Gusev Crater (Parker et al., 2010), have lower northern rims, possibly due to the influence of the topographic dichotomy. Additionally, prior observational investigations of lunar craters have found that low points in the crater rim are frequently aligned with downslope directions in local topography rather than downrange impact direction (Neish et al., 2017, 2014).

It is clear from these studies that antecedent topography influences the crater formation process and potentially the morphology of the impact crater, but these effects are largely unquantified and do not address a common type of antecedent topography: the presence of an older crater. This represents a gap in knowledge about the connection between crater morphology and impact processes, limiting our use of craters as an exploratory tool to probe planetary surfaces. Here, we examine many overlapping, complex lunar craters (Figs. 1, 2) to quantify the influence of antecedent topography on crater morphology. Specifically, we test the hypothesis that crater rims exhibit lower elevations where they overlap antecedent crater basins compared to where they do not. We do so by systematically examining overlapping crater pairs on the lunar surface and determining if crater rims forming in antecedent crater basins are systematically lower relative to the rim that falls outside the antecedent crater. Furthermore, we characterize the magnitude of these differences and establish relationships between rim elevation differences, crater geometry, and the degree of crater overlap.

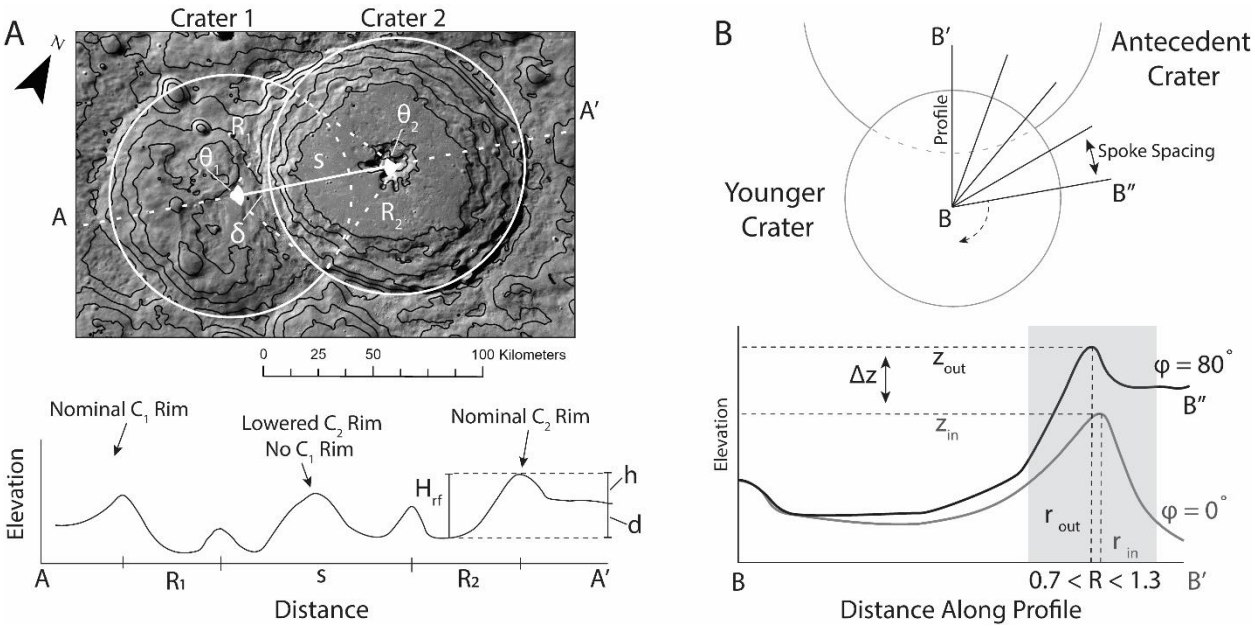

Fig. 1. (A) An overlapping crater pair with 1 km topographic contours overlain on surface imagery (top) and a topographic profile through both craters' centers (bottom). (B) Crater Analysis scheme in plan and profile view. In A, the larger crater (Crater 2) is the younger crater, and the smaller crater (Crater 1) is antecedent to Crater 2. The rim of Crater 2 is ~1 km lower where it overlaps Crater 1. See Supporting Information and Table S1 for mathematical notations.

2. Data & Methods

2.1 Datasets & Crater Pair Selection

We use the Global Lunar DTM 100 (GLD100) for our topographic analysis as it has near-global coverage (79°S - 79°N) of the lunar surface at high spatial resolution (100 m) (Scholten et al., 2012). Among the recent global datasets of lunar craters (Robbins, 2019; Wang et al., 2021), we use the Robbins, 2019 (Robbins, 2019) crater database because it represents a highly complete catalog of lunar craters at least 2 km in diameter, and it provides important characterizations of crater geometry that are necessary for our study. We evaluate only craters with ellipticities (ε) less than 1.3 to avoid the additional complexities and asymmetries associated with oblique impacts and reduce the population of secondary impacts within our analysis (McEwen and Bierhaus, 2006). Our focus on highly circular craters allows us to reduce the complexity of our approach by using the best-fit circular diameter rather than elliptical geometry. We also limit our analysis to craters between 17 and 400 km in diameter (D) to analyze only craters within the complex regime (Pike, 1977). We use the Wide Angle Camera morphology mosaic (Speyerer et al., 2011) for manual relative crater age assessment.

2.2 Determination of Crater Morphometry

For every overlapping crater pair, we extract topographic profiles oriented radially about each crater's centroid. Using these profiles, we examine how crater-rim elevation (z) and distance from the crater centroid (r) change azimuthally (Fig. 1). We perform a preliminary low-resolution survey (profile point spacing of 400 m and a spoke spacing of 10°) on both members of each crater pair to determine their relative ages. Then, we analyze the younger crater with a

point spacing of 100 m and spoke spacing of 5° to produce our final observations. We use a definition of crater rim similar to a recent crater survey of craters on the moon (Wang et al., 2021), selecting the rim to be the maximum-altitude location between 0.7 and 1.3*R*, accommodating craters up to $\varepsilon = 1.3$.

2.3 Crater-Pair Observations

There are several morphometric parameters that we measure to determine which crater in each pair is younger as well as investigate the effects of antecedent topography. Specifically: (1) we measure the peak rim elevation (z) and rim location (r) along each topographic profile; (2) we measure the difference in crater rim elevation between the area inside (z_{in}) and outside (z_{out}) the intersection arc; (3) we measure the degree of overlap between the two craters; and (4) we predict the depth of the older crater relative to the undisturbed surface. We measure the height difference between the rim inside and outside the intersection arc as:

$$\Delta z = \bar{z}_{in} - \bar{z}_{out} \text{ , and} \quad (1)$$

$$\max(\Delta z) = \min(z_{in}) - \bar{z}_{out} . \quad (2)$$

To understand their general relationships, we normalize the difference in rim elevation (Δz or $max(\Delta z)$) by the predicted depth of the older crater (d) based on scaling laws ($d=H_{rf}- h$; Pike, 1977). Where $\Delta z/d = 0$, the rim of the younger crater is not lower where it overlaps the antecedent topography compared to the rim outside this overlap. Negative values of $\Delta z/d$ generally indicate that the rim is lower where it overlaps antecedent topography, and a value of -1 indicates that the rim is lowered by the expected depth of the pristine antecedent crater.

Complex craters are not perfectly cylindrical depressions; therefore, we expect that the $\Delta z/d$ of a crater pair will depend partially on where within the antecedent crater the younger crater rim forms. We measure crater overlap using the distance between the antecedent crater center and the younger crater rim (δ, Fig. 1) and normalize this distance to the older crater radius (R_o). To first order, we expect $max(\Delta z)/d$ to decrease with increasing crater overlap, especially at lower degrees of overlap. If $max(\Delta z)/d$ traces crater topography, it will decrease from near 0 to -1, where the young crater rim forms in the antecedent crater floor. We expect that $\Delta z/d$ will be a less-sensitive tracer of this pattern, as it averages across portions of the young rim that intersect the antecedent rim and collapse terraces. We also examine profiles along rims intersecting antecedent topography to determine how the new rim traces the expected antecedent topography (Fig. 4). Rim elevation difference along individual profiles ($(z - \bar{z}_{out})/d$) is plotted as a function of azimuth normalized to the total intersection arc (φ') to enable averaging across multiple crater pairs. We compare our observations of crater rim topography with the topography of Aristillus Crater (D = 53 km), a relatively pristine, complex crater located on the Lunar nearside (Grier et al., 2001). We measure topography along the perimeter of three circular "craters" (D = 35 km) that intersect Aristillus at distances of s = 21.5, 29.5, and 37.5 km, corresponding to δ values of 0.15, 0.45, and 0.75 R_o, respectively. These measurements provide a proxy for the expected antecedent topography along a crater rim where it would intersect a prototypical complex crater. We normalize elevation along these profiles analogously to the individual rim profiles: $(z-z_{mare})/(z_{mare}-z_{floor})$ using the local mare elevation (z_{mare}) and crater floor elevation (z_{floor}) instead of the exterior rim and predicted crater depth. These comparisons demonstrate how the post-impact rim topography compares to the antecedent topography, how

much of the young rim forms within the antecedent crater floor, and whether the sharp, antecedent terrace-to-floor transition is preserved in the young crater rim.

3. Results & Discussion

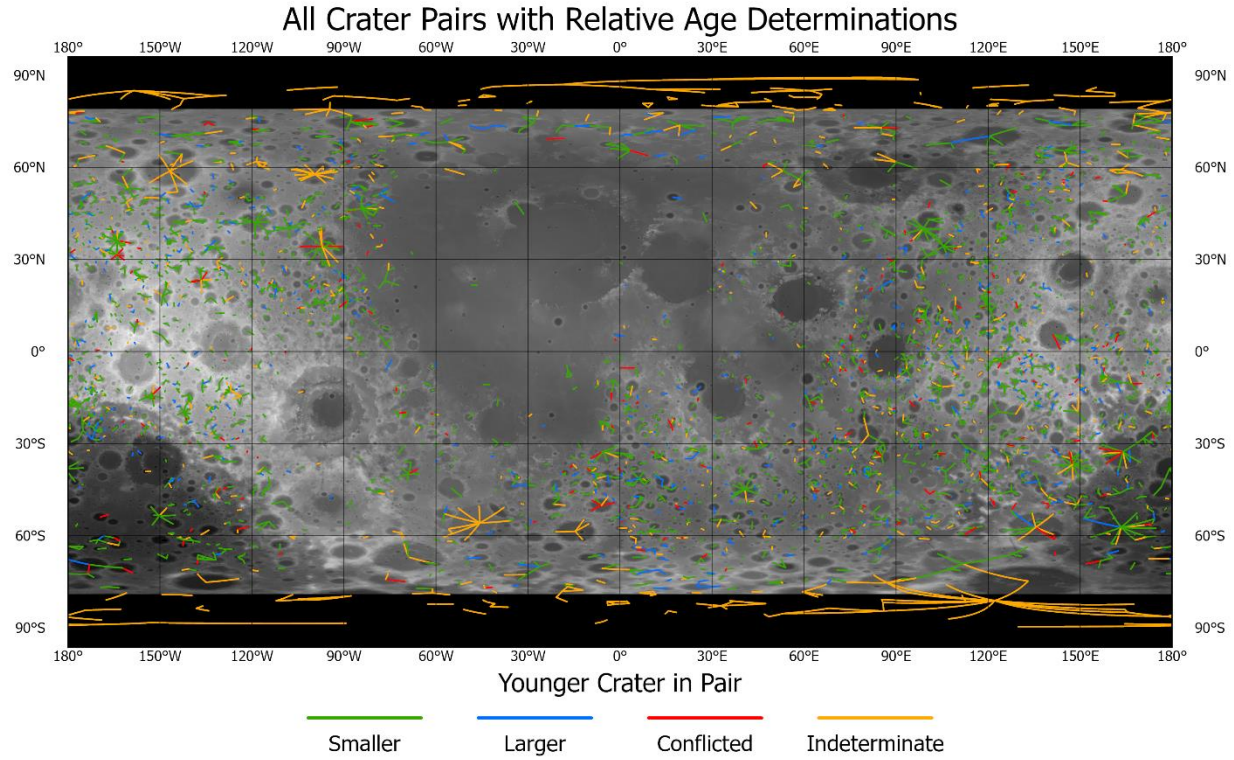

Fig. 2. Overlapping complex crater pairs after filtering and determination of relative age. Lines connect the centers of each crater in the pair with color designating whether the relative age of craters in the pair was determined. Black areas near the poles indicate areas outside the coverage of the topographic dataset (Scholten et al., 2012).

3.1 Crater Pair Determination

Of the ~1.3 million craters in the crater database (Robbins, 2019), 8,653 meet our selection criteria ($\varepsilon < 1.3$, 17 km < D < 400 km), from which we identified 4,932 craters that make 4,024 intersecting crater pairs (*Fig. 2*). These are predominantly found in the highlands due to the overall higher abundance of large ($D > 17$ km) craters. The smaller crater is determined to be younger in 2,482 pairs (61.7%), and the larger crater is determined to be younger in 522 pairs (12.9%). The relative ages of 1,020 (25.3%) pairs could not be determined, of which 393 (9.8%) are caused by insufficient crater overlap (i.e., no topographic profiles intersected the overlapping area) or crater profiles exceeding the data extent near the poles, 404 (10.0%) are indeterminate, and 223 (5.5%) yield conflicting relative ages. Many indeterminate pairs are associated with large craters that have many craters impacting their rims (resulting in a highly variable rim determination) that obscures rim topography in relation to the overlap area of any two crater pairs. On average, the older crater in an overlapping pair has a diameter of ~71 km, and the younger has a diameter of ~35 km.

3.2 Differences in Rim Elevation

We measured the average and maximum rim elevation difference inside and outside the antecedent crater (*Δz* and *max(Δz), Fig. 1*) for the 3,022 crater pairs for which we could determine the relative age. We expect these rim elevation differences to scale with the size of the antecedent relief, so we express elevation differences in terms of the antecedent crater depth (*d*). Center-to-rim distance (*δ, Fig. 1*) informs whether the younger crater rim formed within the antecedent crater floor, or closer to the antecedent rim and is also expected to influence the observed rim elevation difference. Our results show that rim elevation differences are, on average, close to zero where craters minimally overlap ($\delta > 0.8\ R_o$) but decrease as center-to-rim distance decreases (Fig. 3). Average and maximum rim elevation differences decrease approximately linearly until the young crater rim reaches the antecedent crater center ($\delta = 0\ R_o$), at which point the average and maximum rim elevation difference reach values of ~-0.5 and -1 *d*, respectively.

These observations demonstrate that crater rims are generally lower where they intersect the antecedent negative topography of older craters and that the difference in rim elevation scales with both the depth of the older crater and the degree of overlap of the two craters. In cases where the younger crater rim forms in the older crater center ($\delta \sim 0\ R_o$), the lowest part of the intersecting rim is ~1 *d* lower than the exterior rim. However, this is not true for most crater pairs, in which the rim elevation difference is generally less than the antecedent crater depth.

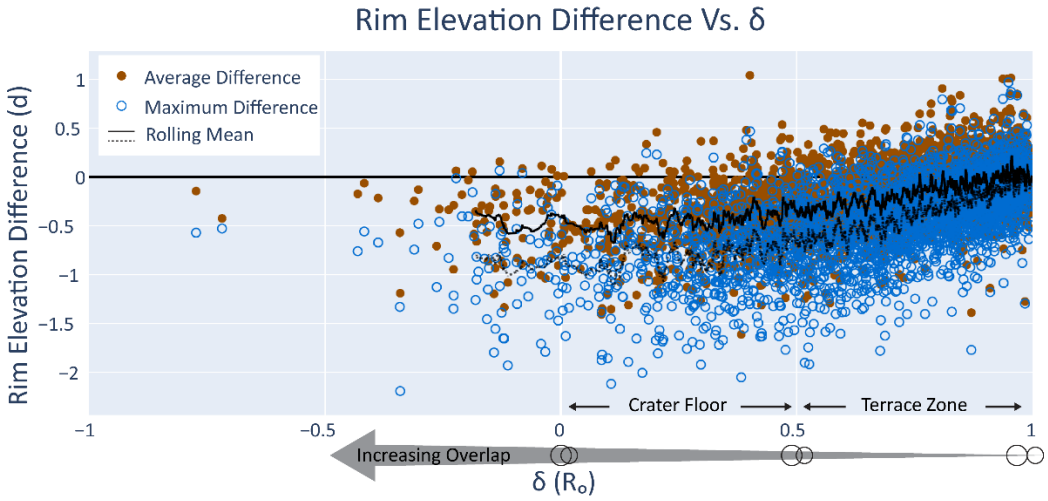

Fig. 3. Average and maximum rim elevation Difference vs. center-to-rim distance (δ) with rolling means for each group. Expected locations of the antecedent crater floor and terrace zone based on scaling laws (Melosh, 1989, p. 198) *and the average older crater diameter (71 km) are marked. In crater pairs with $\delta < 0.5\ R_o$, the young crater rim likely intersects the antecedent flat crater floor. Negative values of δ indicate that the younger crater covers the center of the antecedent crater.*

3.3 Intersecting Rim Shape and Topography

The prior results establish clear end cases: intersecting rims are not lower than exterior rims when craters overlap minimally, and intersecting rims are lower by ~1*d* when craters overlap substantially ($\delta \sim 0\ R_o$). However, the gradual change in rim elevation difference (Fig. 3) does not reflect the shape of the antecedent craters which have a flat crater floor extending to ~0.5 R_o and a sharply rising terrace zone and rim (Melosh, 1989). This indicates that, in some crater pairs, the young crater rim formed within the antecedent crater floor (i.e., at -1 *d*) but is not 1 *d* lower than the exterior rim. To explore the causes of this apparent mismatch, we compare the topography along intersecting crater rims to several profiles of a pristine complex crater that serves as a proxy of antecedent crater topography (Fig. 4). We use Aristillus crater as our model complex crater as it appears relatively pristine and has no intersecting craters within our crater size range.

The antecedent topography proxy (Fig. 4, left side) shows that as craters increase in overlap, the young rim forms deeper into the antecedent basin, with the least overlapping craters (Fig. 4, δ = 0.75 R_o) forming their rims fully within the terrace zone of the antecedent craters. In such cases, we would not expect to see a rim elevation difference equal to the depth of the antecedent crater, because the antecedent topography reaches only half the depth of the antecedent crater floor. However, for moderately and substantially overlapping crater pairs (Fig. 4, δ = 0.45, 0.15 R_o), the antecedent topography clearly flattens and reaches depths of -1 *d* as it reaches the crater floor. For observed crater pairs at these high degrees of overlap (Fig 4, right side), no part of the crater rim reaches an elevation difference of -1 *d*, even at the deepest point of intersection. These observed crater rim profiles also show little flattening at near $\varphi'=0$, though a mild slope break in the most deeply intersecting crater pairs (Fig 4, brown line) may reflect preservation of this antecedent feature. These comparisons reinforce a key finding from Fig. 3: that the rim elevation difference of young crater rims forming in antecedent negative topography is generally less than -1 *d*. The topography of these intersecting crater rims also has less relief than the antecedent topography, but there is evidence that some elements of the antecedent topography (i.e., the slope break corresponding to the terrace-to-floor transition) are preserved.

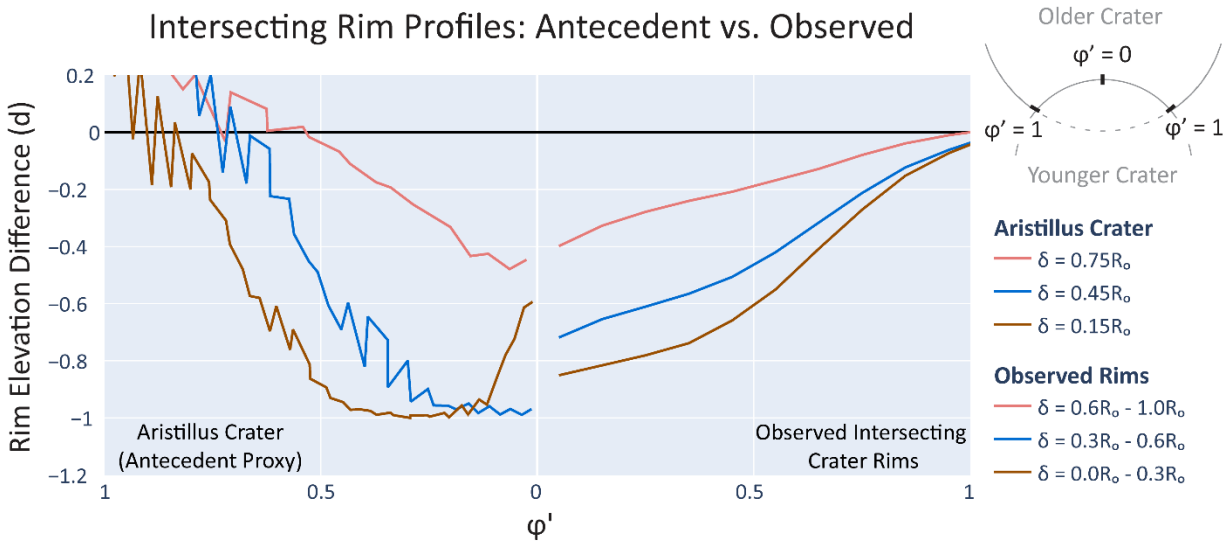

Fig. 4. (Right) Rim elevation difference for individual radial profiles vs. normalized azimuth ($\varphi' = \varphi/(\theta_y/2)$). Data points are binned according to the absolute φ value. (Left) Smoothed topography along a D = 35 km circle intersecting Aristillus Crater (D = 53 km) at various distances: δ = 0.15, 0.45, and 0.75 R_o. Line colors represent crater pairs with less overlap (δ =0.6-1.0 R_o), moderate overlap (δ = 0.3-0.6 R_o), and substantial overlap (δ = 0.0-0.3 R_o). Craters with δ < 0.45 R_o are expected to intersect the flat crater floor, and the observed rim topography is both elevated and smoothed relative to the expected antecedent topography.

3.4 Implications for Crater Formation Processes

These observations show that crater rims are lower where they intersect older craters (Fig. 3), but this lowering is not precisely predicted by the expected antecedent crater depth at the point of rim formation. This mismatch between observed rim lowering and expected antecedent topography provides insight into the way crater formation proceeds in the presence of antecedent topography. To explain these observations, we infer that the younger crater's rim material must have been laterally or circumferentially distributed during crater formation, diffusing the effect of the antecedent negative topography along the rim of the younger crater (Fig. 5). Some of this diffusion may occur during the excavation and uplift stages of crater formation, but the collapse of the transient rim is known to be critical in complex crater rim formation (Melosh and Ivanov, 1999; Senft and Stewart, 2009) and likely plays a larger role. A circumferential distribution of rim materials during transient rim collapse of the younger crater readily explains the observations. First, crater rims are generally not lowered by the full depth of the antecedent crater because circumferentially collapsing materials flow towards the deepest point of intersection. In the crater pairs with the greatest overlap (δ = 0 R_o), we observe cases where the maximum rim elevation difference reaches -1 *d*, demonstrating that there are limits to the extent of this circumferential distribution of material. However, in most cases, this collapse is sufficient to elevate the rim at the deepest point of intersection such that the maximum rim elevation difference is rarely -1 *d*. Second, the circumferential distribution of material during crater formation would effectively smooth the initially sharp relief where the young crater rim intersects the antecedent terrace and rim structures. This explains the observation of smooth, elevated rims relative to the antecedent topography (Fig. 4), in which the floor-to-terrace transition is no longer visible. This smoothing also explains why we see little evidence of positive rim elevation differences where the young crater rim forms close to the antecedent crater rim or antecedent central peak, as these features are not laterally extensive enough to be preserved in the young rim topography.

One caveat to these observations is the role of erosion – both erosion of the antecedent crater before the second impact and erosion of the younger crater after impact into the antecedent. To first order, lunar erosion is well modeled by topographic diffusion (Craddock and Howard, 2000; Fassett and Thomson, 2014), especially on a small scale. However, topographic diffusion may be limited by the slow breakdown of intact rock into regolith, and craters as small as 3 km do not degrade as rapidly as would be predicted from diffusion (Fassett and Thomson, 2014). Erosion of the antecedent crater before impact by the younger crater will not substantially change the key morphometric parameter: the depth of the crater relative to the surrounding terrain. Erosion of the younger crater rim via diffusion would proceed much more rapidly in the radial direction where the curvature is highest, relative to moderate changes in elevation along the crater rim. As

such, the incredibly low yield strength of the collapsing transient crater provides a better explanation for the observed smooth rim profiles rather than post-impact diffusive erosion.

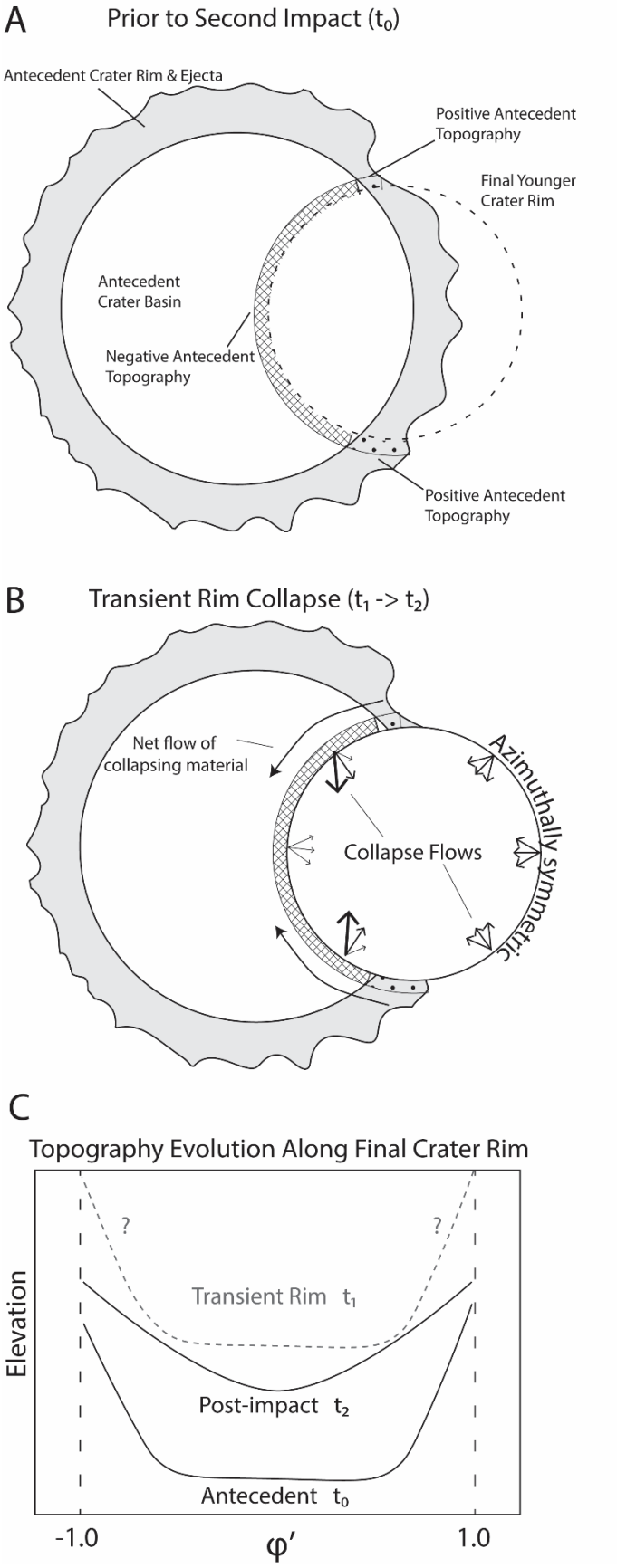
A
Prior to Second Impact (t_0)
Antecedent Crater Rim & Ejecta
Positive Antecedent Topography
Final Younger Crater Rim
Antecedent Crater Basin
Negative Antecedent Topography
Positive Antecedent Topography
B
Transient Rim Collapse (t_1 -> t_2)
Net flow of collapsing material
Collapse Flows
Azimuthally symmetric
C
Topography Evolution Along Final Crater Rim
Elevation
?
?
Transient Rim t_1
Post-impact t_2
Antecedent t_0
-1.0
φ′
1.0

292

Fig. 5. Model of transient rim collapse asymmetries leading to the observed crater morphology. (A) Shows the antecedent topography with indicators of where the new crater will form and the antecedent topography relative to the surrounding terrain, (B) shows the moment of transient rim collapse during the formation of the younger crater, and (C) illustrates the topographic profile along the final crater rim location (Comparable to Figure 4). Asymmetries in the collapse flow cause the rim to collapse towards the antecedent topography, smoothing the final rim profile relative to the antecedent topography.

4. Conclusions

Using the Robbins crater database and a DEM of the lunar surface, we show that antecedent topography influences crater rim topography, and crater rims are systematically lower where they intersect antecedent craters. Additionally, these new crater rims only partially preserve the antecedent topography, and the difference in rim elevation inside and outside the new crater is not equal to the antecedent topographic relief in most cases. From these observations we suggest that transient rim collapse is an important process that may distribute material circumferentially around the new crater rim, leading to the observed shape and relief.

These conclusions formalize and place constraints on the interaction of impact craters with antecedent crater topography, a process that affects ~50% of complex craters on the moon (see Method section) and many others in the solar system. The constraints we place on this interaction, as well as the processes we propose to be responsible, have a bearing on the study of impact craters at large. Our results show that complex craters do not obliterate the underlying topography and that crater rims bear signatures of the topography that preceded them. This incomplete erasure of topography is an important consideration of crater saturation and crater equilibrium(Hirabayashi et al., 2017), which depend sensitively on when craters are rendered unobservable. Additionally, the asymmetric collapse process illustrated in Fig. 5 suggests that the crater rim within the antecedent negative topography may have different geophysical properties compared to other portions of the crater rim. Impact simulations that include the effects of dilatancy (Collins, 2014) suggest that collapsed transient rim materials have some of the highest porosity of materials within the crater basin, notably higher than rim material. Crater rims that form in antecedent topography may, therefore, be more porous than other sections of the crater rim, making them more prone to further modification, changing their gravitational signature, and potentially making them better reservoirs of subsurface fluids. Finally, several Artemis landing sites are on the rims of complex craters with >1 km of height variability and one site (Amundsen Crater Rim (NASA, 2022)) is a very clear case of a complex crater rim forming within the basin of an older, complex, crater. This process of rim formation in overlapping crater pairs is therefore an essential component of the geology of this site, and observations made *in situ* by Artemis astronauts may further our understanding of how antecedent topography alters the crater formation process.

Acknowledgements

Dr. Don Hood was funded by the Baylor Office of the Vice Provost of Research Postdoctoral Scholar program.

Data Availability Statement

The data used in this work are available online via the USGS Astropedia Portal. The Wide Angle Camera (WAC) mosaic, Global Lunar DTM (GLD) 100 Dataset, and Robbins Crater Database are all available for download. Data and code to generate the results we present is archived online via the Texas Data Repository as (Hood et al., 2024) https://doi.org/10.18738/T8/SYWIMY.

Author Contributions:

Don R. Hood: Primary Authorship, Data Analysis, Methodological Development
Brennan W. Young: Data Analysis, Methodological Development, Manuscript Revisions
Aviv L. Cohen-Zada: Manuscript Revisions
Peter B. James: Manuscript Revisions, Science Oversight
Ryan C. Ewing: Manuscript Revisions, Science Oversight
Jeffery S. Lee: Manuscript Revisions, Science Oversight

References

Aschauer, J., Kenkmann, T., 2017. Impact cratering on slopes. Icarus 290, 89–95. https://doi.org/10.1016/j.icarus.2017.02.021

Bramson, A.M., Byrne, S., Putzig, N.E., Sutton, S., Plaut, J.J., Brothers, T.C., Holt, J.W., 2015. Widespread excess ice in Arcadia Planitia , Mars. Geophys. Res. Lett. 42, 1–9. https://doi.org/10.1002/2015GL064844

Collins, G.S., 2014. Numerical simulations of impact crater formation with dilatancy. J. Geophys. Res. Planets 119, 2600–2619. https://doi.org/10.1002/2014JE004708

Craddock, R.A., Howard, A.D., 2000. Simulated degradation of lunar impact craters and a new method for age dating farside mare deposits. J. Geophys. Res. Planets 105, 20387–20401. https://doi.org/10.1029/1999JE001099

Dundas, C.M., Mellon, M.T., Conway, S.J., Daubar, I.J., Williams, K.E., Ojha, L., Wray, J.J., Bramson, A.M., Byrne, S., McEwen, A.S., Posiolova, L.V., Speth, G., Viola, D., Landis, M.E., Morgan, G.A., Pathare, A.V., 2021. Widespread Exposures of Extensive Clean Shallow Ice in the Midlatitudes of Mars. J. Geophys. Res. Planets 126. https://doi.org/10.1029/2020JE006617

Elbeshausen, D., Wünnemann, K., Collins, G.S., 2009. Scaling of oblique impacts in frictional targets: Implications for crater size and formation mechanisms. Icarus 204, 716–731. https://doi.org/10.1016/j.icarus.2009.07.018

Fassett, C.I., Thomson, B.J., 2014. Crater degradation on the lunar maria: Topographic diffusion and the rate of erosion on the Moon: Crater degradation on the lunar maria. J. Geophys. Res. Planets 119, 2255–2271. https://doi.org/10.1002/2014JE004698

Grier, J.A., McEwen, A.S., Lucey, P.G., Milazzo, M., Strom, R.G., 2001. Optical maturity of ejecta from large rayed lunar craters. J. Geophys. Res. Planets 106, 32847–32862. https://doi.org/10.1029/1999JE001160

Hartmann, W.K., Neukum, G., 2001. Cratering chronology and the evolution of Mars, in: Chronology and Evolution of Mars. Springer, pp. 165–194.

Hirabayashi, M., Minton, D.A., Fassett, C.I., 2017. An analytical model of crater count equilibrium. Icarus 289, 134–143. https://doi.org/10.1016/j.icarus.2016.12.032

Hood, D.R., James, P.B., Lee, J., 2023. Compositional and Morphometric Exploration of Van De Graaff Crater on the Lunar Farside, in: Lunar And Planetary Science Conference 2023. p. 1658.

Hood, D.R., Young, B.W., Cohen-Zada, A.L., James, P.B., Ewing, R.C., Lee, J.S., 2024. Supporting Data for "The Effect of Antecedent Topography on Complex Crater Formation." https://doi.org/10.18738/T8/SYWIMY

Izquierdo, K., Sori, M.M., Soderblom, J.M., Johnson, B.C., Wiggins, S.E., 2021. Lunar Megaregolith Structure Revealed by GRAIL Gravity Data. Geophys. Res. Lett. 48. https://doi.org/10.1029/2021GL095978

Krohn, K., Jaumann, R., Elbeshausen, D., Kneissl, T., Schmedemann, N., Wagner, R., Voigt, J., Otto, K., Matz, K.D., Preusker, F., Roatsch, T., Stephan, K., Raymond, C.A., Russell, C.T., 2014. Asymmetric craters on Vesta: Impact on sloping surfaces. Planet. Space Sci. 103, 36–56. https://doi.org/10.1016/j.pss.2014.04.011

McEwen, A.S., Bierhaus, E.B., 2006. The Importance of Secondary Cratering to Age Constraints on Planetary Surfaces. Annu. Rev. Earth Planet. Sci. 34, 535–567. https://doi.org/10.1146/annurev.earth.34.031405.125018

Melosh, H.J., 1989. Impact Cratering: A Geologic Process. Oxford University Press, New York.

Melosh, H.J., Ivanov, B.A., 1999. Impact crater collapse. Annu. Rev. Earth Planet. Sci. 27, 385–415. https://doi.org/10.1146/annurev.earth.27.1.385

NASA, 2022. NASA Identified Candidate Regions for Landing Next Americans on Moon.

Neish, C.D., Herrick, R.R., Zanetti, M., Smith, D., 2017. The role of pre-impact topography in impact melt emplacement on terrestrial planets. Icarus 297, 240–251. https://doi.org/10.1016/j.icarus.2017.07.004

Neish, C.D., Madden, J., Carter, L.M., Hawke, B.R., Giguere, T., Bray, V.J., Osinski, G.R., Cahill, J.T.S., 2014. Global distribution of lunar impact melt flows. Icarus 239, 105–117. https://doi.org/10.1016/j.icarus.2014.05.049

Parker, M.V.K., Zegers, T., Kneissl, T., Ivanov, B., Foing, B., Neukum, G., 2010. 3D structure of the Gusev Crater region. Earth Planet. Sci. Lett. 294, 411–423. https://doi.org/10.1016/j.epsl.2010.01.013

Pike, R.J., 1977. Size-dependence in the shape of fresh impact craters on the Moon, in: Impact and Explosion Cratering: Planetary and Terrestrial Implications. pp. 489–509.

Riedel, C., Minton, D.A., Michael, G., Orgel, C., Bogert, C.H., Hiesinger, H., 2020. Degradation of Small Simple and Large Complex Lunar Craters: Not a Simple Scale Dependence. J. Geophys. Res. Planets 125. https://doi.org/10.1029/2019JE006273

Robbins, S.J., 2019. A New Global Database of Lunar Impact Craters >1–2 km: 1. Crater Locations and Sizes, Comparisons With Published Databases, and Global Analysis. J. Geophys. Res. Planets 124, 871–892. https://doi.org/10.1029/2018JE005592

Scholten, F., Oberst, J., Matz, K.-D., Roatsch, T., Wählisch, M., Speyerer, E.J., Robinson, M.S., 2012. GLD100: The near-global lunar 100 m raster DTM from LROC WAC stereo image data: THE 100 M RASTER DTM GLD100. J. Geophys. Res. Planets 117, n/a-n/a. https://doi.org/10.1029/2011JE003926

Schwenzer, S.P., Abramov, O., Allen, C.C., Bridges, J.C., Clifford, S.M., Filiberto, J., Kring, D.A., Lasue, J., McGovern, P.J., Newsom, H.E., Treiman, A.H., Vaniman, D.T., Wiens, R.C., Wittmann, A., 2012. Gale Crater: Formation and post-impact hydrous environments. Planet. Space Sci. 70, 84–95. https://doi.org/10.1016/j.pss.2012.05.014

Senft, L.E., Stewart, S.T., 2009. Dynamic fault weakening and the formation of large impact craters. Earth Planet. Sci. Lett. 287, 471–482. https://doi.org/10.1016/j.epsl.2009.08.033

Speyerer, E.J., Robinson, M.S., Denevi, B.W., the LROC Science Team, 2011. Lunar Reconnaissance Orbiter Camera Global Morphological Map of the Moon. Lunar Planet Sci Conf 2387.

Wang, Y., Wu, B., Xue, H., Li, X., Ma, J., 2021. An Improved Global Catalog of Lunar Impact Craters (≥1 km) With 3D Morphometric Information and Updates on Global Crater Analysis. J. Geophys. Res. Planets 126, e2020JE006728. https://doi.org/10.1029/2020JE006728

Wünnemann, K., Ivanov, B.A., 2003. Numerical modelling of the impact crater depth-diameter dependence in an acoustically fluidized target. Planet. Space Sci. 51, 831–845. https://doi.org/10.1016/j.pss.2003.08.001